HOM ANALYSIS OF MULTICELL SUPERCONDUCTING CAVITIES

By

John Popielarski

A THESIS

Submitted to
Michigan State University
in partial fulfillment of the requirements
for the degree of

MASTER OF SCIENCE

Department of Electrical and Computer Engineering

2003

Professor Leo Kempel

ABSTRACT

HOM ANALYSIS OF MULTICELL SUPERCONDUCTING CAVITIES

By

John Popielarski

Design of superconducting multi-cell cavities and evaluation of their electromagnetic (EM) properties relies heavily on the use of numerical calculations by computer code. Analysis of the cavity's higher-order modes (HOMs) and its associated power couplers are greatly facilitated by computer simulation. The complete HOM simulation of the Rare Isotope Accelerator (RIA) six-cell 805 MHz for beams traveling about half the speed of light is discussed. RF measurements are essential to verify numerical predictions. The calculations are used, in practice, to design the cavity and perform perturbation studies. The measurements are performed to verify as designed performance. Both are necessary for successful linear accelerator design, especially for superconducting systems. The results of numerical calculations of the EM properties of HOMs are compared to RF measurements on a copper model of a 5-cell superconducting cavity. The EM properties of the fundamental pass-band mode are also compared. The main EM properties of interest are the frequency, shunt impedance and the strength of the coupling to the input coupler. The measurements are done with a bead-pull system and a network analyzer.

ACKNOWLEDGEMENTS

In memory of Heather McPherson

TABLE OF CONTENTS

LIST OF FIGURES

LIST OF TABLES

CHAPTER 1

INTRODUCTION

1.1   Particle acceleration

The early use of particle accelerators in the 1930's became important to the area of nuclear research. Since then, particle accelerators have become important to a widespread area of research and applications. These areas include research in elementary particle physics, nuclear physics, synchotron radiation and medical applications.

Acceleration of particles can be acheived by several methods. The DC voltage of a battery can be used as a simple method to increase the kinetic energy of a particle, where the the kinetic ebergy gained is equal to the electrical energy lost by the battery. Crofton and Walton developed the first mordern accelerator using this method, by charging then disicharging capacitors to achieve a potential difference of 120,000 volts[1]. Other methods, such as the cyclotron, betatron, synchotron and linear accelerators utialize time varying electric and magnetic fields in order to increase the particle's kinetic energy.

The linac is composed of a line of resonent cavities which are intended to give the particle beam energy, accelerating it as it travels down the line. The resonant cavities are powered by RF sources, usually with frequencies in the range of 300-3,000 MHz. The accelerating gap of the RF cavities, a cavity cell, must have the accelerating field pointing in the same direction as the particle beam velocity. This is done by allowing a half of an RF cycle to power the beam. The beam is accelrated with synchronous energy, meaning each time the beam enters a new cell it is timed such that it sees the nominal accelerating field. With the changing velocity of the particle beam as its energy increases, either the cell length or the RF frequency changes in order to maintain synchronous operation. This calls for different cavity designs for each stage of the linac[2].

The main objective of high energy accelrators is to impart a large amount of energy to the particle beam by achieving a high accelerating field in the resonant cavities wtihout a

substantial amount of losses. Reduction of the losses is directly related to the reduction of the surface resistance in the cavity walls. The use of superconductivity greatly reduces the surface resistance of the cavities.

1.2   The Rare Isotope Accelerator

The rare isotope accelerator (RIA) concept is to utilize state-of-the-art superconducting cavities to supply instense beam of exotic isotopes for research in nuclear physics[2]. The linac provides the heavy ions acceleration of up to 400 MeV per nucleon using several different types of superconducting structures. The design of RIA is significantly helped on the experienced gained from the Spallation Nuetron Source (SNS). Part of the RIA linac will use the same accelerating cavities and cryostats produced for the SNS project.

1.3   Design and evaluation of superconducting cavities

While the use of computer simulation greatly facilitates the design of radio frequency (RF) cavities, it is important to confirm simulations with measurements. Much of the highe-order mode (HOM) analysis for the 6-cell cavity was done with *MAFIA* [6]. In this thesis, computer simulation results for a 5-cell axisymmetric copper cavity are compared with RF measurements. The cavity is a prototype of a 6-cell superconducting cavity designed to accelerate beams at 47% the speed of light. The 6-cell cavity is being developed for the Rare Isotope Accelerator (RIA) [3, 4]. Additional *MAFIA* simulations were done for the 5-cell case for comparison with the measurements.

The field profile is measured via a "bead pull" perturbation method in order to calculate R_a/Q_0. The field profile is also used to evaluate the field flatness of the cavity.

Some important HOM properties that are obtained through computational means can also be obtained through bench-top measurements. Quantities that are independent of the cavity material are most desirable because a copper prototype may be used to confirm

simulated results in the design process. There are other important quantities for cavity design, including peak electric and magnetic fields, but they are not readily measured.

1.4   Computer Simulations

MAFIA [6] and *ANALYST* [7] were used for numerical calculation of cavity eigenmodes. Simulations where done on simple 5 and 6-cell (no power couplers or pick-up antennas attached) axisymmetric geometries in 2D. Necessary 3D simulations, such as the design of the power coupler, were done with a single-cell geometry. The simulation results facilitated design the shape and location of the fundamental power coupler (FPC) and confirm that an additional port is not required for a HOM damper.

1.5   Measurements

The measurements were done with a vector network analyzer (VNA) and a bead pull mechanism, as shown in Figure 1.1. Various beads were investigated, including both metallic and dielectric elliptical shaped beads, as well as spherical beads and circular disks. The metallic needle is most sensitve to the axial electric field[9]. Since the axial component of the electric field is the component sought for measurement, the most accurate measurements were acheived with the thin metallic needle, as shown in the inset of Figure 1.1. The thin metallic needle is actually a hyperdermic needle cut to about 7 mm in length. Simple wire antennas of different shapes and sizes were used to couple to different modes. The antennas were mounted on the beam tube end-caps, on which holes were drilled at the center (beam axis) and at various distances off axis, so the bead pull could be placed precisely at the center or at a known distance and angle off axis.

The Q_{ext} is measured in transmission, using the same setup as in Figure 1.1. The FPC antenna has sections of varying lengths, giving the antenna different penetration distances. The input or driven antenna on the right end-cap is made close to match, but more impor-
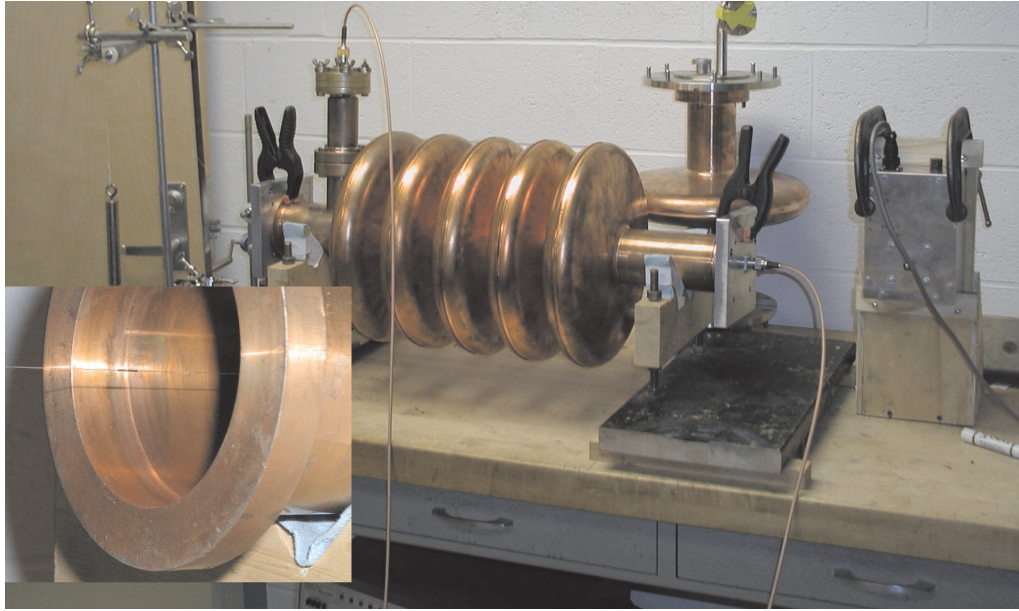
Figure 1.1: Set-up for bead-pull measurements. The input antenna is mounted onto the right end-cap. The power coupler on the left beam tube may be used as a pickup, although an additional antenna on the left end-cap was used in some cases. The inset shows the metallic needle and the fishing line (controlled by the motor on the right) without the end-cap shown in the main picture. The Q_{ext} is measured with the same set-up, adjusting the input antenna for unity coupling.

tantly the input antenna should not disrupt the cavity fields.

CHAPTER 2

THEORY

2.1   Particle acceleration with an RF cavity

A time varying electromagnetic field is used in a linear accelerator to accelerate a particle beam as the beam travels through the cavity. For simplicity, the particle bunch can be represented by an ideal particle of charge q measured in coulombs. The acceleration is achieved by a time rated change in momentum $d\vec{p}/dt$. The equation of motion for the particle is given by

$$\frac{d\vec{p}}{dt} = q(\vec{E} + \vec{v} \times \vec{B}) \tag{2.1}$$

with the momentum $\vec{p} = \gamma m_0 \vec{v}$. The Lorentz factor γ, and the rest mass m_0 of the particle is used to specify $\vec{p}$.

Suppose this change in momentum is achieved along a path where a single component of the electric field, let's say the longitudinal component, is very high compared to other components of the EM fields. The change in momentum p_z is now related to the z component of the electric field (E_z) in a cylindrical coordinate system and its charge q. The particle feels a force along the z direction.

$$F_z = qE_z \tag{2.2}$$

The energy gained by the particle can be determined from the line integral of this force along the path the particle traverses the cavity. It is convenient to define a potential difference the particle sees due to the electric field, the cavity voltage V_C, by evaluating the line integral of E_z along the path the particle travels through the cavity. This cavity voltage is an important figure of merit of a superconducting cavity, and is described in Section 3.4.

2.2 Pill-box modes

The cavity voltage defined in Equation (3.2) relies on the longitudinal, or axial, electric field in the cavity. In order to visualize the EM fields in a cavity, it is relatively straight forward to solve the boundary value problem based on Maxwell's equations for an ideal pillbox cavity. The various solutions to Maxwell's equations are EM field distributions that generally have different resonant frequencies. These solutions are called pill-box modes. Significantly, two types of modes are derived, transverse electric (TE) and transverse magnetic (TM). The different mathematical solutions are denoted by the integer subscripts mnp, referring to the angular, radial and axial variations in the field distributions, e.g. a TM_{110} mode refers to a dipole (one angular variation per $\pi/2$ radians) transverse magnetic (no axial component of the magnetic field) with one radial variation and no axial field variation.

The accelerating mode for cavities are usually the first resonant magnetic monopole, the TM_{010} mode. This mode is called the fundamental mode because it is the first mode in the frequency spectrum. This provides a good means of accelerating the particle as the axial electric field is very high along center axis of the cavity, or the beam axis, and there are no other EM field components along the beam axis.

2.3 Multi-cell elliptical axisymmetric cavities

The accelerating cavity requires the passage of the particle through the cavity. This is done with cylindrical tubes placed along the radial center of the cavity as shown in Figure 2.1. The diameter of these beam tubes are chosen as to not allow the accelerating mode to propagate, i.e. the cut-off frequency of the cylindrical beam tube must be above the frequency of the RF source. The corners of the cavity are of concern when attempting to achieve a high accelerating field for the particle. High surface electric fields near the exit and entrance of the cavity can be dangerous because of their relationship to field emission. High surface magnetic fields have the ability to quench the superconductor.

High accelerating fields are desired along the beam axis of the cavity and high surface fields need to be limited. This can be achieved by perturbing the geometry of the cavity so the beam ports have rounded (elliptical) edges at the iris and along the equator.

Figure 2.1 shows a multi-cell cavity, with a coaxial power coupler. Aside from the coupling ports, the cavity is axisymmetric about the beam axis. The modes in the elliptical cells are classified by analogy to the modes in an ideal pillbox (TM_{mnp} and TE_{mnp} where the subscripts mnp refer to the azimuthal, radial and longitudinal variations). In general, elliptical cavity modes are not necessarily pure transverse magnetic (TM) or transverse electric (TE), although they are more like one or the other. One mode of a single cell cavity splits into 6 pass-band modes in a six cell cavity. Additionally, multi-pole modes have two different polarizations which split in frequency due to asymmetries. The longitudinal electric field of the first six modes, or the TM_{010} passband, for the six-cell cavity have 6 variations. Note that the fundamental mode ($\pi/6$) is no longer the accelerating mode; the accelerating mode is the π-mode.
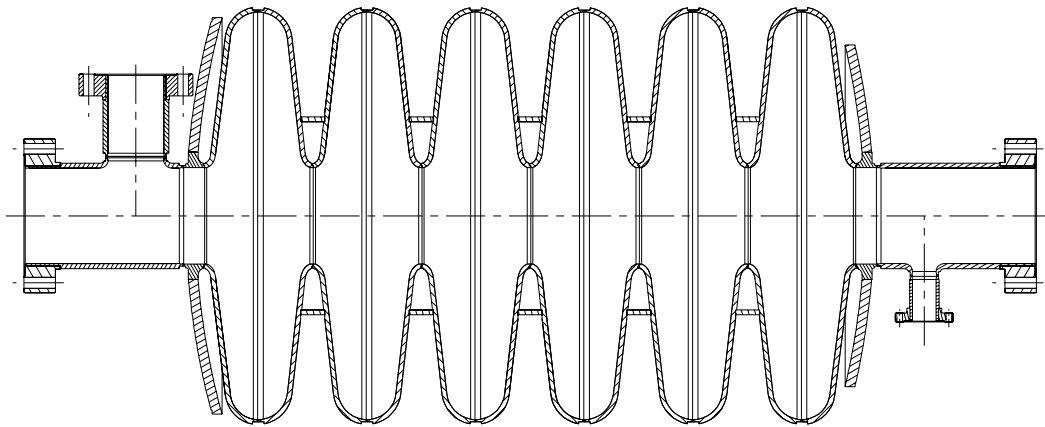

Figure 2.1: Six-cell axisymmetric cavity with power coupler port on the left and pick-up antenna port on the right. The disks on the outside of the endcells attached to the beam tubes are in place to hold the titanium helium vessel and cavity tuner. Stiffening rings are also drawn in place; they are used to maintain the shape of the cavity.

2.4 Perturbation by a metallic object

MAFIA can calculate the relevant mode properties directly from their theoretical definitions. For measurement, manipulation of the theoretical definitions is needed in order to relate the mode properties to the S-Parameters that can be measured with a network analyzer. An important figure of merit, the geometric shunt impedance (R_a/Q_0), which is described in Section 3.5, can be measured with the help of perturbation theory.

Using Slater's perturbation theory, it is possible to calculate the normalized field strength, $\vec{E}_0$ and/or $\vec{H}_0$, by introducing a small metallic perturbation and measuring the change in resonant frequency. A metallic sphere may be used to determine E_z along the beam axis for all TM monopoles, because for these modes the other field components are very small.

For other modes, a metallic needle can be used in combination with a calibration constant. This constant may be derived theoretically [8, 9] or determined experimentally. The metallic needle changes the resonant frequency significantly due only to the presence of an electric field, and the frequency change is greatest when the needle is oriented in the direction of the electric field [9]. With a small change in resonant frequency, $\Delta\omega \ll \omega_o$, Slater's perturbation can be approximated for a sphere by:

$$\Delta\omega = 4\pi\omega_0 a^3 \left(\varepsilon\vec{E}_0^{\,2} - \frac{1}{2}\mu\vec{H}_0^{\,2} \right)$$

(2.3)

where $\vec{E}_0^{\,2}$ and $\vec{H}_0^{\,2}$ are normalized by dividing by twice the cavity's stored energy and a is the radius of the sphere. The technique used herein is a simple method to quickly measure the R_a/Q_0 of a particular mode and compare with *MAFIA*. Therefore, it is only desired to measure the z-component of the electric field on or near the beam axis. A needle was used with calibration through a $TM_{010,\pi}$ measurement with a sphere.

Sphere.

For TM monopole modes, E_z is the only field component along the axis, which simplifies Equation (2.3). The R_a/Q_0 for TM monopoles can be calculated numerically from

$$\frac{R_a}{Q_0} = \frac{\left| \int \sqrt[\pm]{\Delta\omega}\exp\left(i\omega_0 z/c\beta\right) dz\right|^2}{4\pi\varepsilon_0\omega_0^2 a^3},\tag{2.4}$$

allowing us to obtain R_a/Q_0 for a given $c\beta$, or beam velocity, from the bead-pull measurement of $\Delta\omega$ as a function of z.

Needle.

A needle was also used, (see Figure 1.1) to evaluate E_z. Since multi-pole modes have no axial electric field along the beam axis and vary radially, they are measured by moving off axis in the direction corresponding to the strongest coupling: R_a/Q_0 can be determined for any (ρ, ϕ) coordinate. This is done by coupling to the mode with an off-axis antenna and doing the bead-pull 2 cm off axis and $180°$ in rotation from the antenna, where a strong enough signal for a measurement can be found. The two polarizations of the HOMs are measured by rotating the antenna and bead until that the other polarization is coupled (at a different frequency). With a needle of volume $\pi a^2 l$,

$$\frac{R_a}{Q_0} = k\frac{\left| \int \sqrt[\pm]{\Delta\omega}\exp\left(i\omega_0 z/c\beta\right) dz\right|^2}{4\pi\varepsilon_0\omega_0^2 a^2 l},\tag{2.5}$$

The proportionality constant k in Equation (2.5) may be determined experimentally from either a known cavity, such as a pillbox, or from a monopole mode measurement. The R_a/Q_0 results in this paper were obtained from needle measurements, using a proportionality constant obtained from the $TM_{010,\pi}$ mode calibrated with the sphere standard.

CHAPTER 3

FIGURES OF MERIT

3.1 Some important quantities in superconducting cavities

The beam stability can be predicted from the HOM frequency (f), geometric shunt impedance (R_a/Q_0) and coupling strength (Q_{ext}), which are explained in this chapter. The quality factor (Q_0) is also important for the system performance. Because the RF measurements are done on a room temperature copper model of the cavity, its Q_0 is much lower than an actual superconducting niobium cavity. Therefore, a room temperature measurement of Q_0 is not very useful. All of the other quantities were calculated numerically and measured.

3.2 Higher Order Modes

The higher order modes of the cavity is the term used to describe cavity modes that may be excited by the accelerated beam and can become harmful to the beam stability. These are all the modes that are not used to accelerate the beam. In order to determine if the HOM is harmful, an HOM analysis must be done. This includes determining the frequencies of the HOMs and evaluating what type of damage the mode can do to the beam. If the HOM is determined to be harmful, the mode must be damped in order to design a functional cavity.

The RIA 6-cell $\beta = 0.47$ cavity has been designed without a port used specifically for an HOM damper. This is because a HOM analysis was done and very few modes were deemed to be problematic, and those that were will be damped by both the pick-up antenna and the fundamental power coupler. The HOM analysis was done via computer simulation to show this[3].

3.3 Field Flatness

The accelerating mode should have equal energy in each of the cells of the cavity, giving the beam an equal kick from each cell. This gives the cavity a greater accelerating voltage while minimizing peak surface fields. The *field flatness* of the cavity is a measure of how evenly the the energy is distributed in the cavity for the accelerating mode. The field flatness can be described by

$$\frac{\max \Delta |E_z^{peak}|}{\Sigma |E_z^{peakn}|/N}. \tag{3.1}$$

The field flatness, determined from Equation (3.1), is often checked with a bead pull mechanism as in Figure 1.1. Since the square of the electric field is proportional to the change in the resonant frequency, a bead pull measurement using a thin metallic needle is suitable to record the square of the longitudinal electric field in each cell. The $\Delta |E_z^{peak}|$ is the greatest change in the maximum $|E_z|$ between any two cells, and the $\Sigma |E_z^{peakn}|/N$ is the average maximum $|E_z|$ across all the cells.

3.4 Geometric Shunt Impedance

The shunt impedance and quality factor of the superconducting cavity are two important figures of merit. Both of these depend on the surface resistance of the cavity walls. Dividing the shunt impedance by the quality factor gives a useful material-independent quantity (R_a/Q_0). The R_a/Q_0 of a cavity mode is an integral of the longitudinal electric field (E_z). For TM monopole modes, E_z exists along the beam axis, where the other electric and magnetic field components are very small. For all other modes, E_z goes to zero along the beam axis. Since beam instabilities [5] can occur due to any mode with non-zero E_z on or near the axis, it is important to calculate R_a/Q_0 for modes other than the accelerating mode.

The quality factor of the cavity is the ratio of the stored energy in the cavity times the angular frequency to the power dissipated in the cavity walls. The power dissipated, P_c,

is dependent on the surface resistance, R_s, of the cavity walls. The shunt impedance is determined from the average voltage seen by the beam, V_c, and the dissipated power, P_c. The beam voltage is calculated from the longitudinal electric field along the beam axis ($a = 0$), for monopole modes, or near the beam axis ($a \neq 0$) for multi-pole modes:

$$V_C = \left| \int_0^d E_z \left(\rho = a, z \right) \exp\left(\frac{i\omega_0 z}{c\beta} \right) dz \right|, \tag{3.2}$$

where ω_o is the resonant angular frequency of the mode, $c\beta$ is the velocity of the beam, d is the total length of the cavity, and ρ is the radial cylindrical coordinate. Thus, V_C is the integral of the longitudinal force on a particle traveling at the speed $c\beta$, accounting for the time and space dependence in the field. The particle travels on the crest of the wave by making the cell length $\frac{1}{2}\beta\lambda$, thus the particle passes through the cell on $1/2$ of an RF cycle. The shunt impedance (linac definition) is given by

$$R_a = \frac{V_C^2}{P_C}. \tag{3.3}$$

3.5   Cavity Coupling Strength

The coupling strength of the power coupler is determined from the external quality factor (Q_{ext}). The Q_{ext} of the accelerating mode must be small enough to accommodate the beam loading of the accelerating mode; the Q_{ext} of the HOMs determine the rate of damping of beam induced fields in the HOMs and hence the beam stability. The Q_{ext} calculations for multi-cell cavities can be difficult because simulations require large mesh sizes due the to larger structure and the asymmetric geometry. However, a 3D code can be used to calculate the single cell Q_{ext} for each mode. Multi-cell modes can be more easily calculated with 2D meshes; the 2D calculation give an energy ratio (the ratio of the total stored energy to the energy in the cell adjacent to the coupler). Multiplying the Q_{ext} of the single cell cavity mode by the energy ratio for each multi-cell mode in the multi-cell pass-band provides an

adequate approximation of the multi-cell Q_{ext} values. If all of the cells have the same energy, the 6-cell Q_{ext} is 6 times the single cell Q_{ext}. This method requires a knowledge of which single cell mode corresponds to each multi-cell passband. This can be determined by viewing graphical simulation results, but it is not always straightforward.

The external quality factor, Q_{ext}, is a ratio of the stored energy times ω_o to the power emitted out of the power coupler. If other losses are assumed to be small, the overall Q of the cavity, the loaded Q, (Q_L), can be expressed in terms of Q_0 and Q_{ext} only; it is measured with the VNA from the bandwidth of the resonance. Typically, operational values of Q_{ext} are very large for superconducting cavities, i.e. the coupling is weak. The Q_{ext} can be determined from Q_L via a measurement of the transmission coefficient (S_{21}). With unity coupling (matched load),

$$Q_{ext} \quad = 2Q_L/|S_{21}|^2 \tag{3.4}$$

If the input antenna does not have unity coupling, a correction factor may be determined from the reflection coefficient (S_{11}). It is preferred to be near unity coupling in order to minimize systematic errors in the measurement.

3.6 Peak surface fields

The average accelerating field, E_{acc}, is the field the beam sees during its passage through the cavity. Using Equation (3.2) to determine V_c along the trajectory of the beam, E_{acc} is the ratio of the cavity volatage to the length of the cavity. In order to minimize undesireable effects from high surface fields, the ratios of peak surface fields to the accelerating field should be minimized. The peak electric field is determined from computer simulation; these peak fields are near the iris of the ellipical cavities and are not easily measured. For the peak magnetic field, the peak field is near the equator of the elliptical cavity.

CHAPTER 4

SIMULATIONS AND MEASUREMENTS OF A 5-CELL PROTOTYPE

4.1   Field profiles and R_a/Q_0

MAFIA was used to calculate the E_z profiles on or near the beam axis for all relevant HOMs [3]. Figure 3 compares two *MAFIA* profiles with the measured profiles. The mode classification is determined from the field distribution, a step which is also required to predict the multi-cell Q_{ext}, as explained in Section 1.1.

Figures 3a and 3b show the raw data collected: the S_{21} phase shift ($\Delta\phi$) as a function of bead position. The bead position is determined by measuring the distance and time of the bead travel. The S_{21} phase shift is proportional to the change in resonant frequency due to the perturbation. The frequency change is calculated from the phase shift by interpolating a measurement of phase as a function of frequency for the unperturbed cavity mode. Using a conducting needle (radius = 0.25mm, length = 6.34 mm), the maximum $\Delta\phi$ was about 7° for the $TM_{010,\pi}$ mode (Figure 3a), which corresponds to 3.00 kHz change in frequency. For the $TM_{010,\pi/5}$ mode (Figure 3b), the conducting needle was placed off-axis 2 cm, and the maximum phase change was only about 1.2°, corresponding to a Δf_{max} of 574 Hz. Figures 3c and 3d show a comparison of *MAFIA* to the measurements. Prior measurements were done with the conducting sphere, and the calibration constant k was determined to be 1.15 from the monopole measurement. Data manipulation is needed to account for a change in the direction of the E_z field (e.g. the field changes direction four times in Figure 3c) and then R_a/Q_0 can be numerically calculated from Equation (2.5) with the calibration constant. The results are shown in Table 1.

The cavity is designed to accelerate the beam from $\beta = 0.40$ to $\beta = 0.52$, where βc is the beam velocity. Hence, the dependence of R_a/Q_0 on β is of interest. Figure 4.2a shows the dependence of the measured R_a/Q_0 on β, as obtained via Equation (2.4). *MAFIA*
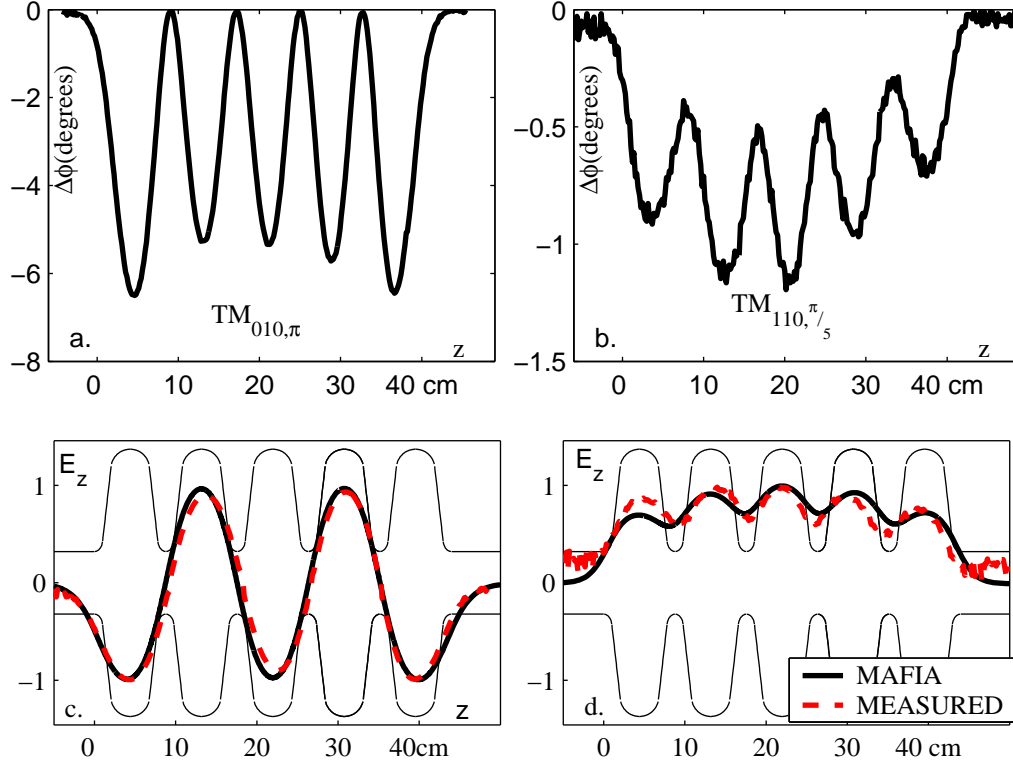
Figure 4.1: (a) Raw data collected for the accelerating mode along the beam axis from a metallic needle perturbation. (b) Data collected for a dipole mode 2 cm off axis. (c,d) Comparison of normalized E_z profiles, taken from the measurements in (a,b).

Table 4.1: Summary of measured and simulated frequencies and shunt impedances. The listed R_a/Q_0 values are the maximum values in the range $0.40 \leq \beta \leq 0.52$. The dipole modes were evaluated at a radius of 2 cm.

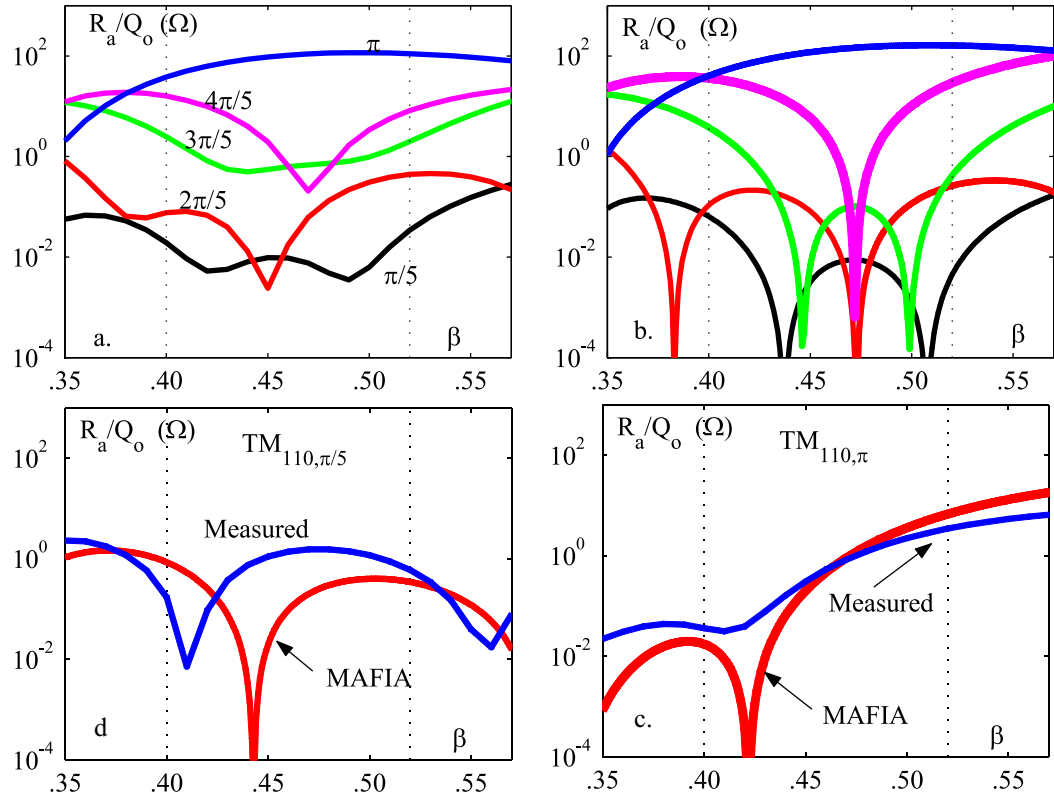| Mode	Frequency (MHz)		R_a/Q_o (Ω)	
	Simulated	Measured	Simulated	Measured
$TM_{010,\pi/5}$	794.0	794.4	.0652	.0431
$TM_{010,2\pi/5}$	797.0	797.7	.268	.515
$TM_{010,3\pi/5}$	800.6	801.5	3.94	3.28
$TM_{010,4\pi/5}$	803.5	804.7	37.8	25.6
$TM_{010,\pi}$	804.7	805.8	162.2	156.4
$TM_{110,\pi}$	1133	1132	6.744	3.984
$TM_{110,4\pi/5}$	1139	1140	13.095	26.47
$TM_{110,3\pi/5}$	1147	1149	7.130	5.202
$TM_{110,2\pi/5}$	1156	1158	3.534	5.577
$TM_{110,\pi/5}$	1161	1164	.8562	1.542

Figure 4.2: The measured (a) and simulated (b) R_a/Q_0 as a function of beam velocity for the fundamental passband. The figures illustrate the misalignment of the measured data due to inaccurate displacement measurements, which can lead to large disagreement with the simulation results for certain discrete points. Graphs (c) and (d) compare two modes in the the TM_{110} pass-band.

was also used to calculate the dependence on β via Equations (3.2) and (3.3) and the results are shown in Figure 4.2b. The maximum R_a/Q_0 was used when evaluating beam stability issues [3]. Because the locations of the zeros rely heavily on exact bead displacement measurements, measuring the maximum R_a/Q_0 over the range of interest gives better agreement without a complicated set-up.

4.2   Coupling measurements

The measurement of Q_{ext} is done on the accelerating mode in order to design the input coupler. The Q_{ext} can be calculated from Equation (3.4) and measurements of Q_L and the *S*-Parameters. The VNA is connected to the power coupler and an antenna in the beam tube. The antenna is constructed such that it is close to a matched load.

Calculation of Q_{ext} for a single cell cavity was done in [3] using *ANALYST*. *MAFIA* could also be used to compute Q_{ext} using the procedure in [10]. The multi-cell Q_{ext} was computed from 2D *MAFIA* simulations. The predicted Q_{ext} for some HOMs are presented in Table 4.2.

Table 4.2: Summary of measured and simulated coupling strengths. The energy ratio is of the total energy to the energy in the end cell. The simulated 5-cell Q_{ext} values were calculated by multiplying the simulated energy ratios by the simulated Q_{ext}.

	Frequency (MHz)		Ratio	$Q_{ext,5-cell}$	
Mode	Simulated	Measured	Simulated	Simulated	Measured
$TM_{010,single}$	805.0	799.7	–	2.170×10^6	2.820×10^6
$TM_{010,\pi/5}$	794.0	794.4	23.75	5.154×10^7	3.116×10^7
$TM_{010,2\pi/5}$	797.0	797.7	6.817	1.479×10^7	1.040×10^7
$TM_{010,3\pi/5}$	800.6	801.5	3.744	8.124×10^6	6.266×10^6
$TM_{010,4\pi/5}$	803.5	804.7	2.839	6.161×10^6	4.480×10^6
$TM_{010,\pi}$	804.7	805.8	5.319	1.115×10^7	6.380×10^6
$TM_{020,single}$	1725	1725	–	3.410×10^5	4.420×10^5
$TM_{020,\pi/5}$	1702	1703	10.93	3.727×10^6	2.773×10^6
$TM_{020,2\pi/5}$	1712	1713	3.828	1.305×10^6	3.816×10^5
$TM_{020,3\pi/5}$	1726	1728	3.055	1.042×10^6	2.805×10^5
$TM_{020,4\pi/5}$	1741	1743	4.280	1.459×10^6	3.579×10^5
$TM_{020,\pi}$	1752	1754	13.17	4.491×10^6	1.250×10^6
$TM_{110,1cell}$	1154.70	1149.5	–	9.580×10^5	1.090×10^6

CHAPTER 5

DISCUSSION

5.1 Analysis of error

The measured results in Tables 1 and 2 provide good agreement with the simulated results for the fundamental pass-band. However, there are significant discrepancies in R_a/Q_0 at certain velocities. The Q_{ext} measurements are in good agreement for the multi-cell pass-band modes and single cell modes, while HOM dipoles do have a discrepancy.

The R_a/Q_0 measurements were all done with a calibrated needle, although measurements with a conducting sphere should provide accurate results for monopole modes.

The measured Q_{ext} values were generally lower than the simulated values. The energy distribution could be affected by the input coupler. This could, in effect, lower the expected energy ratio as simulated in the ideal case with *MAFIA*. The measured profiles of the HOMs evaluated without the penetrating input coupler did have good agreement, corresponding to an energy ratio agreement in the vicinity of $\pm 10\%$. The energy ratios in the presence of the penetrating input coupler were not evaluated.

Several modes were simulated for the 6-cell cavity [3]. All the monopole, dipole, quadrupole, and sextupole modes below their cut-off frequencies (both TM and TE) were simulated using an axisymmetric geometry. The R_a/Q_0, energy ratios, single-cell Q_{ext} and frequencies were all considered to identify possible problematic modes.

Simple RF measurements were done on a copper model of a superconducting cavity at room temperature to confirm some key RF properties. Though the results presented in this thesis provide reasonable agreement with the simulation results, more accurate measurements are possible, although this would require additional equipment and more complicated set-ups.

The measurements of the field profile could be improved with an automated system, such a PC connected to the VNA and an electronic displacement sensor, simultaneously

taking measurements. Additionally, the path of the bead should be parallel to the beam axis. The bead can deviate from this path if the guides on the ends of the cavity are not properly aligned.

The computer simulations provided accurate results and were a great facilitator in the development of the 6-cell cavity, and the RF measurements provided a good confirmation of the simulations.

CHAPTER 6

CONCLUSION AND FUTURE WORK

6.1   Conclusion

This work described in this thesis was required to develop an elliptical cavity that is to be part of the RIA linac where the beam travels around half the speed of light. The computer simulation of the of the cavity indicated the cavity design was acceptable and should be used in the RIA linac. RF measurements confirmed the results of the computer simulation.

Currently, two power couplers have been designed, constructed and tested for niobium prototype cavities. Soon to be assembled is test cryo-module that will hold the two cavities as if they were a part of the linac, and tested under realistic high-power conditions.

6.2   Future work

My future plans are to utilize the experience gained while doing this research and design, build and test a new concept superconducting cavity. The fundamentals learned established a good background in the field of cavity design that will be an invaluable tool in accelerator physics.

BIBLIOGRAPHY

[1] Edwards DA and Syphers M J 1993 An Introdutionto the Physics of High Energy Accelerators (New York: JohnWiley and Sons) p 19

[2] Shepard K W, Delayen J R, Lyneis C M, Nole J, Ostroumov P, Staples J W, Brawly J, Hovater C, Kedzie M, Kelly M P, Mammasser J, Piller C, Portillo M 1999 SC Driver Linac for a Rare Isotope Facility in Proccedings of the 9th Workshop on RF superconductivity, Report LA-13782-C, LANL, Los Alamos, New Mexico p 345-351

[3] Grimm T, Hartung W, Marti F, Podlech H, York R C, Popielarski J, Wiess C, Kempel L, Ciovati G, Kneisel P 2002 Input Coupling and Higher-Order Mode Analysis of Superconducting Cavities for the Rare Isotope Accelerator in Proceedings of the Eight European Particle Accelerator Conference (Geneva: EPS-1GA Publishing) p. 2241

[4] Compton C C, Grimm T L, Hartung W, Podlech H, York R C, Ciovati G, Kneisel P, Barni D, Pagani C, Pierini P 2001 Niobium Development for the High-Energy Linac of the Rare Isotope Accelerator in Proceedings of the 2001 Particle Accelerator Conference (Piscataway, New Jersey: IEEE Publishing) p. 1044

[5] Padamsee H, Knobloch J and Hays T 1998 RF Superconductivity for Accelerators (New York: John Wiley & Sons, Inc.) p 154

[6] Mafia 4, Computer Simulation Technology, Darmstadt, Germany (http://www.cst.de)

[7] Analyst, Simulation Technology & Applied Research, Inc., Wisconsin, USA (http://www.staarinc.com)

[8] Maier L C and Slater J C Field Strength Measurements in Resonant Cavities 1952, Journal of Applied Physics, Vol 23, p 68-77

[9] Ginzton E L 1957 Microwave Measurements (New York: McGraw-Hill) p 446

[10] Balleyguier P 1998 External Q Studies for APT SC-Cavity Couplers in Proceedings of the XIX International Linac Conference (Argonne, Illinois: ANL-98128) p. 133